Mode-Symmetry-Assisted Optical Pulling by Bound States in the Continuum

Hang Li,[1] Yongyin Cao,[1,*] Rui Feng,[1] Bojian Shi,[1] Yuzhi Shi,[2] Yang Chen,[3] Dongliang Gao,[4] Tongtong Zhu,[5] Donghua Tang,[6] Fangkui Sun,[1] Cheng-Wei Qiu,[7,†] and Weiqiang Ding[1,8,‡]

[1]*Institute of Advanced Photonics, School of Physics, Harbin Institute of Technology, Harbin 150001, China*
[2]*Institute of Precision Optical Engineering, School of Physics Science and Engineering, Tongji University, Shanghai 200092, China*
[3]*Chinese Academy of Sciences Key Laboratory of Mechanical Behavior and Design of Materials, Department of Precision Machinery and Precision Instrumentation, University of Science and Technology of China, 230027 Hefei, China*
[4]*School of Physical Science and Technology, Collaborative Innovation Center of Suzhou Nano Science and Technology, Soochow University, Suzhou 215006, China*
[5]*School of Optoelectronic Engineering and Instrumentation Science, Dalian University of Technology, Dalian 116024, China*
[6]*Department of Physics, School of Science, Northeast Forestry University, Harbin 150040, China*
[7]*Department of Electrical and Computer Engineering, National University of Singapore, 4 Engineering Drive 3, Singapore 117583, Singapore*
[8]*Collaborative Innovation Center of Extreme Optics, Shanxi University, Taiyuan 030006, China*

(Received 15 October 2023; accepted 20 May 2024; published 20 June 2024)

Aside from optical pushing and trapping that have been implemented successfully, the transportation of objects backward to the source by the optical pulling forces (OPFs) has attracted tremendous attention, which was usually achieved by increasing the forward momentum of light. However, the limited momentum transfer between light and object greatly constrains the amplitudes of OPFs. Here, we present a mechanism to generate strong interactions between object and background through the bound states in the continuums, which can generate large OPFs without increasing the forward momentum of light. The underlying physics is the extraction of momentum from the designed background lattice units assisted by mode symmetry. This work paves the way for extraordinary optical manipulations and shows great potential for exploring the momenta of light in media.

DOI: 10.1103/PhysRevLett.132.253802

Light usually transports objects forward due to the positive radiation pressure when it acts upon an object [1,2]. Recently, the optical pulling forces (OPFs), which drag objects toward the source direction, have attracted widespread attention due to their fascinating physics and potential applications [3–28]. From the perspective of momentum conservation, the key point to get pushing-pulling forces is to break the forward-backward symmetry and redistribute the momentum of scattering light [29,30]. Therefore, the mainstream method to obtain OPFs is to increase the forward momentum of light, for instance, using structured light fields with off-axial momentums that may be redirected to the axial direction when scattered by objects [3,14,15,18].

Despite those extensive studies, however, the efficient generation of OPFs is still constrained by harsh restrictions on the light beams and/or objects [18,19,29]. It is predicted that the background engineering should also be an alternative scheme for OPF [4,31]. For instance, in a dielectric interface, a plane wave can generate a pulling force on macroscopic objects by amplifying the momentum of photons when light is scattered from one medium into another with a higher refractive index [5,23]. Interestingly, through the topological structure engineering of light momentum in the background, robust OPFs can also be obtained by a plane wave [10,24,32]. However, in all these configurations, the forward momentum enhancement still plays the key rule, constrains the amplitude of the pulling force, and also lacks flexibility.

In this Letter, we propose an elegant mechanism to realize large OPFs inspired by the driving force of maglev trains, which is distinguished from the background-enabled OPFs mentioned above, where the forward momentum enhancement of light was still the key factor. The new physics reported here lies in the mode-symmetry-dependent interaction, which is akin to the distributed propulsive forces experienced by maglev trains. For the first time, we realized large and long-range OPFs in the case of optical total reflection, which demonstrates the explicit utilization of background momentum, but not the forward momentum enhancement of light used in previous research. Here, the used mode is the bound states in the continuums (BICs), which have attracted extensive attention due to their advantages in strong light confinement and potential applications [33–47]. It is noted that, although some works have explored the optical forces in strong resonant

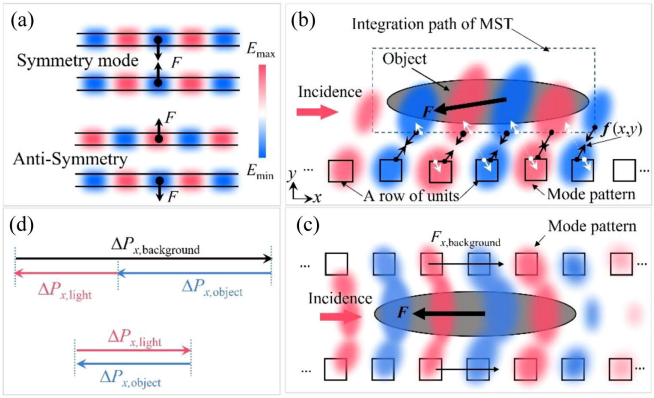

FIG. 1. Schematic of optical pulling force assisted by mode symmetry. (a) The attractive force by the symmetry mode (upper part), and the repulsive force cause by the antisymmetry mode (lower part). (b) When an object is placed near a row of discrete units (the open squares), an OPF may be realized provided the mode pattern is excited properly. The white and black arrows illustrate the repulsive-attractive force elements on an integrating path of Maxwell's stress tensor surrounding the object (the dashed rectangle). In the y direction, however, the object is unstable and will be dragged toward the units. (c) Stable pulling is obtained by the distributed pulling forces of each unit in a double-array structure, while the pushing force acting on the surrounding units is expected. (d) Explicit momentum transfer among light, object, and background lattice occurred in the current optical pulling mechanism (upper part), rather than limited between light and object only used in previous researches (lower part). In this case, even if the momentum of light decreases also (such as being reflected), OPF is still possible due to the introduction of background momentum, and the force amplitude may be large.

structures and using BIC modes [48–55], the key points are quite different from the present work. Those works mainly utilized the resonance generated strong localizations of light, which naturally results in enhanced optical trapping or deforming of objects (unit cells or isolated spheres, cylinders, and nanorods) [48–55], but not for efficient OPF generation.

Figure 1 illustrates the principle of the operation. As shown in Fig. 1(a), optical modes excited in nanophotonic structures can induce attractive (symmetric mode, upper part) or repulsive (antisymmetric mode, lower part) forces between them [56–58]. Suppose an object is set near a row of units fixed on the substrate, it can experience an OPF even in the case of plane wave incidence, provided the mode symmetry is excited and engineered properly, as shown in the Fig. 1(b). In this case, the background units contribute to the pulling force due to the engineered mode symmetry, as illustrated by the force elements (white and black arrows). However, the pulling is unstable in the y direction (will be dragged toward the array), and long-range operation is also challenging. More information about the characteristics of optical pulling force on the object near the single array units can be found in Sec. I in Supplemental Material [59].

Inspired by the stable and long-distance traveling maglev train, we envision to form a double array to realize long range and stable OPFs, as shown in Fig. 1(c). Because of the lateral symmetry, the net force along the y direction will be canceled out, and the object will be pulled stably. More importantly, since there is a strong interaction between the object and the background units, the forward momentum enhancement of light is not required anymore, which is the necessary condition to obtain OPF in previous research, as illustrated in Fig. 1(d). Now, the linear momentum transfer is among the three bodies of light, object, and the background units [upper part of Fig. 1(d)], but not between light and object only as before [lower part of Fig. 1(d)]. From Fig. 1(d), one can also find that the limitation on the amplitude of OPF is loosed. Now, two key factors remain: (1) how to form a lossless light channel by only a double array, and (2) how to extract the background momentum into optical manipulation, and (3) how to switch the mode symmetry synchronously to keep a continuous pulling when the object moving through.

Here, Fabry-Pérot (FP)-BICs mode is found to be the best candidate to fix the above two key factors properly, due to the perfect localization of light inside the channel. We use the following parameters to demonstrate the results quantitatively, i.e., $n_a = 3.55$, $n_b = 1.33$, $l = 160$ nm, $a_x = 2.25\ l$, and $a_y = 2.2a_x$. The band structure of TM polarization is calculated and shown in Fig. 2(a), where the gray region above the light line means light can radiate into the surrounding medium. We then calculate the quality factor (Q) for the second and the third bands by using eigenmode analysis [66] and find three modes of $\mathrm{BIC}_{1,2,3}$ having huge Q factors, as shown in Fig. 2(b), which means that the leaky modes gradually evolve into BICs modes and light is trapped in the channel perfectly. The insets in Fig. 2(b) show the field distributions of $|E_z|^2$ for the three BICs modes, respectively. It is seen clearly that these guided modes are all well confined in the structure. The BIC_3 mode is concentrated inside the unit array, which is an at-Γ BICs mode with a zero k_x. The $\mathrm{BIC}_1(\mathrm{BIC}_2)$ mode is an off-Γ BIC mode and satisfies the transverse Fabry-Pérot resonance condition of $k_y a_y = n\pi$ with $n = 1(n = 2)$. More information about the characteristics of the FP-BIC mode can be found in Sec. II in Supplemental Material [59].

Now, we place an ellipsoid dielectric object in the centerline of the channel and excite the BIC modes from the left port. The refractive index of the object is $n = 1.75$, and the radii of the object in the x and y axis are $r_x = 1.8$ μm and $r_y = 0.2$ μm, respectively. The optical force on the object can be calculated by integrating the Maxwell stress tensor (MST) on a closed contour surrounding the object, i.e.,

$$\langle \boldsymbol{F} \rangle = \oint_s \left\langle \overleftrightarrow{\mathbf{T}} \right\rangle \cdot \mathbf{n} dS, \tag{1}$$

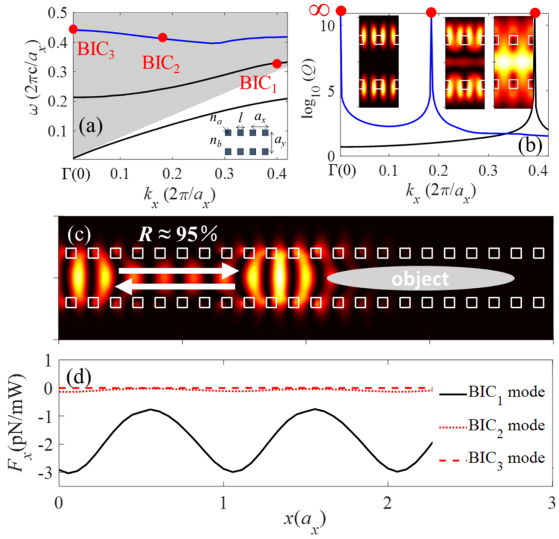

FIG. 2. Characteristics of the BIC modes and corresponding pulling forces. (a) Band structure of the double-array units for the TM mode. Parameters of the double-array units: $n_a = 3.55$, $n_b = 1.33$, $l = 160$ nm, $a_x = 2.25\ l$, and $a_y = 2.2a_x$. The normalized frequencies (with unit $2\pi c/a_x$) marked by $\mathrm{BIC}_{1,2,3}$ are $\omega_1 = 0.3273$, $\omega_2 = 0.4119$, $\omega_3 = 0.4422$, respectively. (b) Q factor for the second and the third bands. The values for the modes of $\mathrm{BIC}_{1,2,3}$ tend to infinite. The insets show the distributions of $|E_z|^2$ of BIC modes. (c) Distribution of $|E_z|^2$ (BIC_1 mode) when the object is introduced in the channel. The small square array shows the units and the larger ellipse is the object. The incident energy is almost totally reflected ($R \approx 95\%$). (d) For the BIC_1 mode, the maximum force exerted on the object exceeds -3 pN/mW. The forces induced by the BIC_2 and BIC_3 modes are very small due to the weak light distributions inside the channel.

$$\langle \overleftrightarrow{\mathbf{T}} \rangle = \frac{1}{2}\mathrm{Re}\left[\mathbf{D}\otimes\mathbf{E}^* + \mathbf{B}\otimes\mathbf{H}^* - \frac{1}{2}\overleftrightarrow{\mathbf{I}}(\mathbf{D}\cdot\mathbf{E}^* + \mathbf{B}\cdot\mathbf{H}^*)\right], \tag{2}$$

where $\langle\cdot\rangle$ means the time average over an oscillation period; $\otimes$ stands for dyadic operation; $\mathbf{n}$ is the normal unit vector of the closed surface S, and $\overleftrightarrow{\mathbf{I}}$ is the unit tensor.

Figure 2(c) shows that the BIC_1 mode in the channel is almost completely reflected by the object ($R \approx 95\%$). Usually, a total reflection gives a maximum pushing force. Here, OPFs exceeding -3 pN/mW are obtained, as shown in Fig. 2(d), which is more than one order of magnitude larger than those obtained in previous mechanisms [3,10,13,18,25,67]. In case of the BIC_2 mode, the optical forces are also negative. However, the amplitude is very small due to the weak localizations of the light field inside the channel (mainly localized in the units). The BIC_3 mode is a regular symmetry protected at Γ BICs without propagation momentum along the x direction, and the force acting on the object tends to zero, as expected. The scattered field distributions of BIC_2 and BIC_3 modes by the object are shown in Sec. III Supplemental Material [59] for reference.

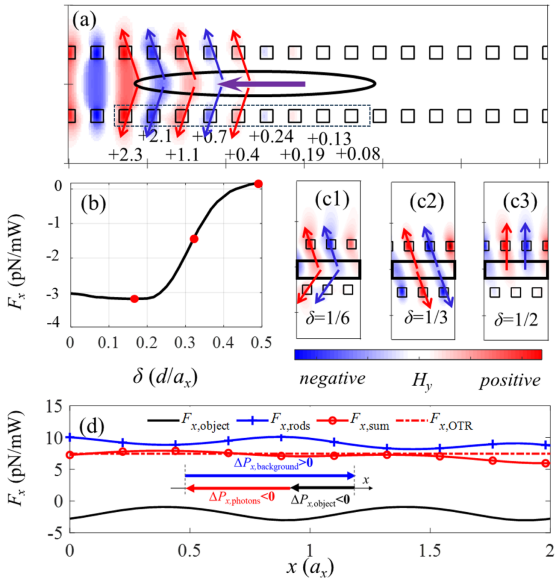

FIG. 3. Physical origin of the enhanced OPFs. (a) Distributed OPFs on the object. The distribution of H_y is also shown for clarity. The red and blue arrows symbolize the attractive forces between the units and the object (the repulsive forces between the object and the background units are not shown here for simplicity). The purple arrow represents the net force on the object. The numbers below the unit cells show the optical forces (the x components) on the corresponding unit cell (in units of pN/mW). (b) Maximum pulling forces on the object at different misalignments $\delta = d/a_x$. (c1)–(c3) Distributions of H_y at $\delta = 1/6$, $1/3$, and $1/2$, respectively. (d) Optical forces and linear momentum conservation in the system. The black solid curve is the OPFs on the object, $F_{x,\mathrm{objects}}$. The blue line (with "+") is the force on the unit cells $F_{x,\mathrm{units}}$. The red line (with "o") shows the sum of $F_{x,\mathrm{sum}} = F_{x,\mathrm{objects}} + F_{x,\mathrm{units}}$, which is consistent with the force calculated by the linear momentum conservation in case of optical total reflection, $F_{x,\mathrm{OTR}}$. The inset shows the linear momentum conservation between light, object, as well as background units.

To investigate the physical origins of these large OPFs, we plot the magnetic field distribution of H_y around the object in Fig. 3(a). Here, the optical attraction by the mode symmetry between the object and the surrounding units is depicted. Since the x components of attractive forces on the object are all negative, a net large OPFs on the object is obtained naturally. Although the BIC_1 mode is robust to the misalignment δ, the pulling force of the BIC_1 mode exerted on the object changes sensitively, as shown in Fig. 3(b). This is because the contribution from the upper- and lower-unit arrays could be canceled out in case of misalignment, as shown in Fig. 3(c). For instance, when the misalignment is $\delta = 1/3$, the top and bottom layers both have attractive forces, but in opposite directions. Therefore, the total force on the object is reduced greatly compared to the case of $\delta = 0$ in Fig. 3(a).

To understand the role of the background units more comprehensively, we explore the momenta transfer in the OPFs. When the incident mode is almost totally reflected by the object, the momentum change of light is $\Delta P_{x,\mathrm{light}} \approx -2P_{x,\mathrm{inc}} < 0$. The negative OPFs mean the object also gets a negative impulse of $\Delta P_{x,\mathrm{object}} < 0$. According to linear momentum conservation, an extra momentum must be balanced by the units of the background units, and large OPFs on the discrete grating units is expected.

To verify this viewpoint, we calculate the forces on the units near the object, as shown in Fig. 3(d). The net forces on these units are all positive. When adding the optical forces on the object and those on the discrete units, we find the total force $F_{x,\mathrm{sum}}$ is consistent with the force caused by light momentum decrease in case of total reflection ($F_{x,\mathrm{OTR}}$), i.e., the momentum conservation relation is

$$\begin{aligned}&\Delta P_{\mathrm{object}} + \Delta P_{\mathrm{photons}} + \Delta P_{\mathrm{background}} \\ &= (F_{x,\mathrm{object}} + F_{x,\mathrm{rods}} + F_{x,\mathrm{OTR}})\Delta t \\ &= 0. \end{aligned} \tag{3}$$

It is evident that the background units explicitly participate in the interaction between light and object, and the momentum transfer in this procedure is among the light, object, and background units. It is noted that the discrete feature of the unit array is vital to extract background momentum because the longitudinal component of light momentum on a planar slab is conservative, as demonstrated in Sec. IV of Supplemental Material [59].

Notably, the elliptical particle is chosen to clarify the interaction between the object and the background units. In reality, it is shown that the optical pulling forces are almost immune to the particle size and shape (Sec. V of Supplemental Material [59]). The mechanism reported here provides a new road map for extracting background momentum into long-range optical manipulation, which is beneficial for manipulating arbitrarily shaped objects. What is more, the bidirectional transport can be realized easily by switching the polarization of the incident source (Sec. VI of Supplemental Material [59]).

When a particle passes through the channel, it causes reflection and scattering loss transforming the BIC mode into a quasi-BIC mode. To measure the effect of the quasi-BIC quantitatively, Fig. 4(a) shows the maximum pulling force on the object with the tuning of a_y and the incident frequency ω. The Q factor is the appropriate parameter to measure the deviation from perfect BIC condition, which can also be tuned by a_y or ω, and the results are shown in Figs. 4(b) and 4(c), respectively. From the cases of $Q = 500$, 1000, 5000, and ∞, one can observe that the magnitudes of OPFs depend on the resonant strength of the structure. Interestingly, even in the case of the small Q factor of $Q = 500$, the amplitudes of OPFs are still larger than those reported previously [13,67]. These results show

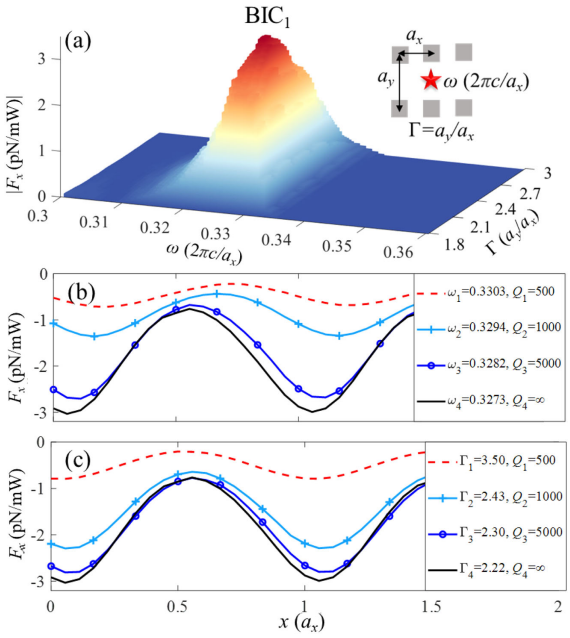

FIG. 4. Changes of the OPFs with the resonant strength (Q factor). (a) 3D map of $|\max(F_x)|$ exerted on the object as a function of incident frequency ω and the width a_y. Other parameters are the same as those in Fig. 3. (b) Changes of OPFs with resonant strength through selecting proper incident frequency, while the width of $a_y = 2.22\ a_x$ is fixed. (c) The same as (b) except for by tailoring a_y and keeping the frequency of $\omega = 0.3273\ 2\pi c/a_x$ fixed.

that the OPF achieved by this strategy is very efficient and robust to parameter deviations.

Based on the above analysis, we can attribute the large OPFs to the interaction between the object and discrete background units, akin to the distributed propulsion of a maglev train through the magnetic poles between the train and the track. In this scenario, the momenta of the background units play a crucial role in the OPFs and explicitly contribute to the linear momentum conservation among the object, light, and background. This mechanism stands apart from previous mechanisms, which focus on the forward momentum enhancement of light. Notably, the OPFs demonstrated here greatly exceed the magnitudes observed in prior studies by more than one order of magnitude and represent a general mechanism valid in various BICs systems (see Sec. VII in Supplemental Material [59]) and for various particle shapes (Sec. VIII in Supplemental Material).

In summary, we have demonstrated a novel mechanism for achieving large and long-range OPFs. The underlying physics hinges on the symmetry-dependent interaction forces between the object and the background units, facilitating the transfer of linear momentum among the object, incident light, and background. This contrasts with previous investigations, which primarily focused on momentum transfer between the object and the incident

light alone. Additionally, we have showcased the resilience of OPFs to variations in system parameters. For the first time, we have harnessed the BICs mode to enable long-range optical manipulation, distinct from traditional forms of force enhancement and optical trapping in BICs systems. The principles and findings presented in this study open new avenues for optical manipulations and provide fresh insights into the interplay between light and matter.

This work was supported by National Natural Science Foundation of China (Grant No. 12274105), the Heilongjiang Natural Science Funds for Distinguished Young Scholar (Grant No. JQ2022A001), the Fundamental Research Funds for the Central Universities (HIT.OCEF.2021020, 2023FRFK06007), and the joint guidance project of Natural Science Foundation of Heilongjiang Province (Grant No. LH2023A006). The authors thank the HPC Studio at Physics School of Harbin Institute of Technology for access to computing resources through INSPUR-HPC@PHY.HIT.

*Corresponding author: yycao@hit.edu.cn
†Corresponding author: chengwei.qiu@nus.edu.sg
‡Corresponding author: wqding@hit.edu.cn

[1] A. Ashkin, Phys. Rev. Lett. **24**, 156 (1970).
[2] I. Levchenko, K. Bazaka, S. Mazouffre, and S. Xu, Nat. Photonics **12**, 649 (2018).
[3] J. Chen, J. Ng, Z. Lin, and C. T. Chan, Nat. Photonics **5**, 531 (2011).
[4] A. Dogariu, S. Sukhov, and J. J. Sáenz, Nat. Photonics **7**, 24 (2013).
[5] V. Kajorndejnukul, W. Ding, S. Sukhov, C.-W. Qiu, and A. Dogariu, Nat. Photonics **7**, 787 (2013).
[6] J. J. Sáenz, Nat. Photonics **5**, 514 (2011).
[7] V. Shvedov, A. R. Davoyan, C. Hnatovsky, N. Engheta, and W. Krolikowski, Nat. Photonics **8**, 846 (2014).
[8] C. E. M. Démoré, P. M. Dahl, Z. Yang, P. Glynne-Jones, A. Melzer, S. Cochran, M. P. MacDonald, and G. C. Spalding, Phys. Rev. Lett. **112**, 174302 (2014).
[9] A. V. Maslov, Phys. Rev. Lett. **112**, 113903 (2014).
[10] H. Li, Y. Cao, B. Shi, T. Zhu, Y. Geng, R. Feng, L. Wang, F. Sun, Y. Shi, M. A. Miri, M. Nieto-Vesperinas, C. W. Qiu, and W. Ding, Phys. Rev. Lett. **124**, 143901 (2020).
[11] J. Lu, H. Yang, L. Zhou, Y. Yang, S. Luo, Q. Li, and M. Qiu, Phys. Rev. Lett. **118**, 043601 (2017).
[12] D. B. Ruffner and D. G. Grier, Phys. Rev. Lett. **109**, 163903 (2012).
[13] T. Zhu, Y. Cao, L. Wang, Z. Nie, T. Cao, F. Sun, Z. Jiang, M. Nieto-Vesperinas, Y. Liu, C. W. Qiu, and W. Ding, Phys. Rev. Lett. **120**, 123901 (2018).
[14] A. Novitsky, C.-W. Qiu, and A. Lavrinenko, Phys. Rev. Lett. **109**, 023902 (2012).
[15] A. Novitsky, C.-W. Qiu, and H. Wang, Phys. Rev. Lett. **107**, 203601 (2011).
[16] V. G. Shvedov, A. V. Rode, Y. V. Izdebskaya, A. S. Desyatnikov, W. Krolikowski, and Y. S. Kivshar, Phys. Rev. Lett. **105**, 118103 (2010).
[17] S. Sukhov and A. Dogariu, Phys. Rev. Lett. **107**, 203602 (2011).
[18] X. Li, J. Chen, Z. Lin, and J. Ng, Sci. Adv. **5**, eaau7814 (2019).
[19] E. Lee and T. Luo, Sci. Adv. **6**, eaaz3646 (2020).
[20] R. Jin, Y. Xu, Z. G. Dong, and Y. Liu, Nano Lett. **21**, 10431 (2021).
[21] L. Lin, P. S. Kollipara, A. Kotnala, T. Jiang, Y. Liu, X. Peng, B. A. Korgel, and Y. Zheng, Light Sci. Appl. **9**, 34 (2020).
[22] D. E. Fernandes and M. G. Silveirinha, Phys. Rev. A **91**, 061801(R) (2015).
[23] C.-W. Qiu, W. Ding, M. R. C. Mahdy, D. Gao, T. Zhang, F. C. Cheong, A. Dogariu, Z. Wang, and C. T. Lim, Light Sci. Appl. **4**, e278 (2015).
[24] A. Ivinskaya, N. Kostina, A. Proskurin, M. I. Petrov, A. A. Bogdanov, S. Sukhov, A. V. Krasavin, A. Karabchevsky, A. S. Shalin, and P. Ginzburg, ACS Photonics **5**, 4371 (2018).
[25] A. Mizrahi and Y. Fainman, Opt. Lett. **35**, 3405 (2010).
[26] A. Minopoli, S. Wagner, E. Erben, W. Liao, I. D. Stoev, E. Lauga, and M. Kreysing, eLight **3**, 16 (2023).
[27] I. D. Stoev, B. Seelbinder, E. Erben, N. Maghelli, and M. Kreysing, eLight **1**, 7 (2021).
[28] O. Brzobohatý, V. Karásek, M. Šiler, L. Chvátal, T. Čižmár, and P. Zemánek, Nat. Photonics **7**, 123 (2013).
[29] H. Li, Y. Cao, L.-M. Zhou, X. Xu, T. Zhu, Y. Shi, C.-W. Qiu, and W. Ding, Adv. Opt. Photonics **12**, 288 (2020).
[30] W. Ding, T. Zhu, L.-M. Zhou, and C.-W. Qiu, Adv. Opt. Photonics **1**, 024001 (2019).
[31] Y. Shi, Q. Song, I. Toftul, T. Zhu, Y. Yu, W. Zhu, D. P. Tsai, Y. Kivshar, and A. Q. Liu, Appl. Phys. Rev. **9**, 031303 (2022).
[32] R. Jin, Y. Xu, Z.-G. Dong, and Y. Liu, Nano Lett. **21**, 10431 (2021).
[33] C. W. Hsu, B. Zhen, J. Lee, S. L. Chua, S. G. Johnson, J. D. Joannopoulos, and M. Soljacic, Nature (London) **499**, 188 (2013).
[34] Y. Chen, H. Deng, X. Sha, W. Chen, R. Wang, Y. H. Chen, D. Wu, J. Chu, Y. S. Kivshar, S. Xiao, and C. W. Qiu, Nature (London) **613**, 474 (2023).
[35] X. Zhang, Y. Liu, J. Han, Y. Kivshar, and Q. Song, Science **377**, 1215 (2022).
[36] K. Koshelev, S. Kruk, E. Melik-Gaykazyan, J.-H. Choi, A. Bogdanov, H.-G. Park, and Y. Kivshar, Science **367**, 288 (2020).
[37] C. Huang, C. Zhang, S. Xiao, Y. Wang, Y. Fan, Y. Liu, N. Zhang, G. Qu, H. Ji, and J. Han, Science **367**, 1018 (2020).
[38] Y. Zeng, G. Hu, K. Liu, Z. Tang, and C. W. Qiu, Phys. Rev. Lett. **127**, 176101 (2021).
[39] Y. Zhang, A. Chen, W. Liu, C. W. Hsu, B. Wang, F. Guan, X. Liu, L. Shi, L. Lu, and J. Zi, Phys. Rev. Lett. **120**, 186103 (2018).
[40] W. Ye, Y. Gao, and J. Liu, Phys. Rev. Lett. **124**, 153904 (2020).
[41] D. C. Marinica, A. G. Borisov, and S. V. Shabanov, Phys. Rev. Lett. **100**, 183902 (2008).
[42] W. Liu, B. Wang, Y. Zhang, J. Wang, M. Zhao, F. Guan, X. Liu, L. Shi, and J. Zi, Phys. Rev. Lett. **123**, 116104 (2019).
[43] F. Monticone and A. Alù, Phys. Rev. Lett. **112**, 213903 (2014).

[44] T. Zhu, Y. Shi, W. Ding, D. P. Tsai, T. Cao, A. Q. Liu, M. Nieto-Vesperinas, J. J. Sáenz, P. C. Wu, and C.-W. Qiu, Phys. Rev. Lett. **125**, 043901 (2020).
[45] C. W. Hsu, B. Zhen, A. D. Stone, J. D. Joannopoulos, and M. Soljačić, Nat. Rev. Mater. **1**, 16048 (2016).
[46] B. Wang, W. Liu, M. Zhao, J. Wang, Y. Zhang, A. Chen, F. Guan, X. Liu, L. Shi, and J. Zi, Nat. Photonics **14**, 623 (2020).
[47] Z. Chen and M. Segev, eLight **1**, 2 (2021).
[48] J. Zhang, K. F. MacDonald, and N. I. Zheludev, Opt. Lett. **39**, 4886 (2014).
[49] C. B. Rojas Hurtado, J. Dickmann, F. Feilong Bruns, T. Siefke, and S. Kroker, Opt. Express **28**, 20106 (2020).
[50] E. N. Bulgakov and A. F. Sadreev, Opt. Lett. **45**, 5315 (2020).
[51] E. N. Bulgakov, K. N. Pichugin, and A. F. Sadreev, Phys. Rev. A **102**, 043518 (2020).
[52] H. Qin, Y. Shi, Z. Su, G. Wei, Z. Wang, X. Cheng, A. Q. Liu, P. Genevet, and Q. Song, Sci. Adv. **8**, eade7556 (2022).
[53] V. Liu, M. Povinelli, and S. Fan, Opt. Express **17**, 21897 (2009).
[54] S. Yang, C. Hong, Y. Jiang, and J. C. Ndukaife, ACS Photonics **8**, 1961 (2021).
[55] E. N. Bulgakov and A. F. Sadreev, Phys. Rev. B **106**, 165430 (2022).
[56] M. A. Miri, M. Cotrufo, and A. Alu, Opt. Lett. **43**, 4104 (2018).
[57] G. S. Wiederhecker, L. Chen, A. Gondarenko, and M. Lipson, Nature (London) **462**, 633 (2009).
[58] P. T. Rakich, M. A. Popović, M. Soljačić, and E. P. Ippen, Nat. Photonics **1**, 658 (2007).
[59] See Supplemental Material at http://link.aps.org/supplemental/10.1103/PhysRevLett.132.253802, which includes Refs. [60–65], for additional information about the charcteristic of BIC mode and the detailed discussion of the optical pulling force.
[60] R. Gomez-Medina, M. Laroche, and J. J. Sáenz, Opt. Express **14**, 3730 (2006).
[61] S. Fan, W. Suh, and J. D. Joannopoulos, J. Opt. Soc. Am. A **20**, 569 (2003).
[62] C. W. Hsu, B. Zhen, S.-L. Chua, S. G. Johnson, J. D. Joannopoulos, and M. Soljačić, Light Sci. Appl. **2**, e84 (2013).
[63] W. Yan, R. Faggiani, and P. Lalanne, Phys. Rev. B **97**, 205422 (2018).
[64] B. Zhen, C. W. Hsu, L. Lu, A. D. Stone, and M. Soljacic, Phys. Rev. Lett. **113**, 257401 (2014).
[65] E. N. Bulgakov and D. N. Maksimov, Phys. Rev. Lett. **118**, 267401 (2017).
[66] W. Yan, R. Faggiani, and P. Lalanne, Phys. Rev. B **97**, 205422 (2018).
[67] T. Zhu, A. Novitsky, Y. Cao, M. R. C. Mahdy, L. Wang, F. Sun, Z. Jiang, and W. Ding, Appl. Phys. Lett. **111**, 061105 (2017).